Dalton Transactions

Accepted Manuscript

ROYAL SOCIETY OF CHEMISTRY

www.rsc.org/dalton

Journal Name

RSCPublishing

ARTICLE

Heptanuclear lanthanide [Ln_7] clusters: from blue-emitting solution-stable complexes to hybrid clusters

Cite this: DOI: 10.1039/xoxxoooooox

Angelos B. Canaj,[a] George K. Tsikalas,[a] Aggelos Philippidis,[b] Apostolos Spyros,[a,]* and Constantinos J. Milios[a,]*

Received ooth January 2012,
Accepted ooth January 2012

DOI: 10.1039/xoxxoooooox

www.rsc.org/

The use of LH_3 (2-(β-naphthalideneamino)-2-hydroxymethyl-1-propanol) and aibH (2-amino-isobutyric acid) in 4*f* chemistry has led to the isolation of eight new isostructural lanthanide complexes. More specifically, the reaction of the corresponding lanthanide nitrate salt with LH_3 and aibH in MeOH, under solvothermal conditions in the presence of NEt_3, led to the isolation and characterization of seven complexes with the general $[Ln^{III}_7(OH)_2(L')_9(aib)]\cdot 4MeOH$ formulae (Ln= Gd, **1**·4MeOH; Tb, **2**·4MeOH; Dy, **3**·4MeOH; Ho, **4**·4MeOH; Er, **5**·4MeOH; Tm, **6**·4MeOH; Yb, **7**·4MeOH L'= the dianion of the Schiff base between naphthalene aldehyde and 2-amino-isobutyric acid). Furthermore, the isostructural Y^{III} analogue, cluster $[Y^{III}_7(OH)_2(L')_9(aib)]\cdot 4MeOH$ (**8**·4MeOH) was synthesized in a similar manner to **1**-**7**. The structure of all eight clusters describes a distorted $[M^{III}_6]$ octahedron which encapsulates a seventh M^{III} ion in an off-centre fashion. Dc magnetic susceptibility studies in the 5 – 300 K range for complexes **1**-**7** reveal the presence of dominant antiferromagnetic exchange interactions within the metallic clusters as evidenced by the negative Weiss constant, θ, while ac magnetic susceptibility measurements show temperature and frequency dependent out-of-phase signals for the $[Dy^{III}_7]$ analogue (**3**·4MeOH), suggesting potential single molecule magnetism character. Furthermore, for complex **1**, simulation of its *dc* magnetic susceptibility data yielded very weak antiferromagnetic interactions within the metallic centres. Solid-state emission studies for all **1**-**8** clusters display ligand-based emission, while extended 1-D and 2-D NMR studies for **8**·4MeOH reveal that the species retain their structural integrity in solution. In addition, TGA measurements for **1, 3** and **7** revealed excellent thermal stability up to 340 °C for the clusters.

Introduction

In the last few years the synthesis and studies of lanthanide-based clusters have entered with great potential in the field of molecular magnetism. While in the past such species were mainly synthesized and studied with respect to their emission properties, as light emitting diodes, optical fibres, lasers, optical amplifiers, NIR-emitting materials and sensory probes,[1] 4*f* clusters have recently gained a great deal of attention as single molecule magnets (SMMs), *i.e.* species that can retain their magnetization once magnetized in the absence of an external magnetic field.[2] This is mainly due to their intrinsic magnetic properties originating from both large magnetic moments and spin-orbit coupling based magnetic anisotropy (with the exceptions of La^{III}, Gd^{III} and Lu^{III}), which are the main prerequisites for the establishment of the SMM behavior. Since the first 4*f*-based SMM reported in 2003 with a barrier for the relaxation of the magnetization of ~ 330 K,[3] many lanthanide clusters have been found to display analogous behavior,[4] while nowadays impressive barriers of up to ~810 K[5] and 842 K[6]

have been reported, given of course that an Arrhenius analysis is valid on such systems. Given both the remarkable electronic and magnetic properties of the 4*f* ions, we recently embarked on a project towards the synthesis of "hybrid"-dual molecular species that would display both magnetic and electronic-optical properties,[7] since such molecules would be at the interface of magnetism and electronics-optics. More specifically, we aim at the synthesis of such species, with the ultimate goal being the investigation of how one property may (or may not) affect the other. Herein, we report the syntheses, structures, magnetic properties and emission properties of seven new homometallic heptanuclear lanthanide clusters and their Y^{III} analogue, bearing a new Schiff-base that was synthesized *in situ* upon reacting naphthalene aldehyde and the artificial amino acid 2-amino-isobutyric acid (Scheme 1), in the presence of lanthanide ions. Furthermore, the solution stability of the clusters was investigated *via* NMR studies on the diamagnetic Y^{III} analogue. Finally, all clusters display thermal stability up to ~ 340 ^{o}C, a rare feature for polynuclear lanthanide cages. A small part of this work has been previously communicated.[8]

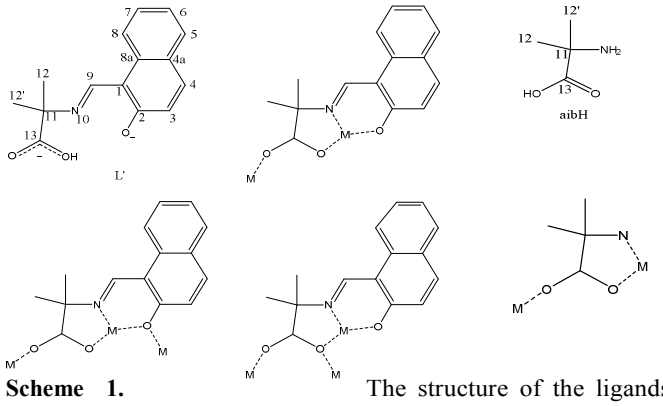

Scheme 1. The structure of the ligands discussed in the text and their coordination modes in **1** - **8**. Numbers referrer to the C, H labelling in the NMR spectra.

Experimental Section

Materials and physical measurements

All manipulations were performed under aerobic conditions, using materials as received. Elemental analyses (C, H, N) were performed by the University of Ioannina microanalysis service. Variable-temperature, solid-state direct current (dc) magnetic susceptibility data down to 2.0 K were collected on a Quantum Design MPMS-XL SQUID magnetometer equipped with a 7 T DC magnet at the University of Crete. Diamagnetic corrections were applied to the observed paramagnetic susceptibilities using Pascal's constants. Powder XRD measurements were collected on freshly prepared samples of **1**, **2**, **4**, **5**, **6, 7** and **8** on a PANalytical X'Pert Pro MPD diffractometer at the University of Crete. ^{1}H and ^{13}C 1D and 2D NMR spectra of **8** in $CDCl_3$ solution were obtained on a Bruker Avance III 500 MHz spectrometer at the University of Crete, using standard instrument software and pulse sequences. Solid state absorbance spectra were recorded on a Perkin Elmer Lambda 950 UV/Vis spectrometer, with a step of 2 nm and area 250-800 nm. Solid state Fluorescence spectra were recorded on a Jobin-Yvon Horiba, Fluoro Max-P (SPEX) fluorescence spectrometer with excitation from a Xenon arc lamp.

Syntheses

General synthetic strategy applicable to **1-8***:*
To colourless solutions of the corresponding $Ln(NO_3)_3{\cdot}6H_2O$ ($Y(NO_3)_3{\cdot}6H_2O$ for **8**) in MeOH were added equivalent amounts of aibH, LH_3 and NEt_3. The solutions were then transferred to Teflon-lined autoclaves and kept at 120 ^{o}C for 14 hours. After slow cooling to room temperature single crystals of the general formulae $[M^{III}_7(OH)_2(L')_9(aib)]{\cdot}4MeOH$ (M= Gd, **1**·4MeOH; Tb, **2**·4MeOH; Dy, **3**·4MeOH; Ho, **4**·4MeOH; Er, **5**·4MeOH; Tm, **6**·4MeOH; Yb, **7**·4MeOH Y, **8**·4MeOH; L'= the dianion of the Schiff base between naphthalene aldehyde and 2-amino-isobutyric acid) were obtained in ~ 25-40 % yields, washed with Et_2O and dried in air.
Elemental Anal. calcd (found) for dried **1** solvent free: C 47.47 (47.55), H 3.15 (3.41), N 3.98 (3.89); **2**: C 47.31 (47.18), H 3.14 (3.45), N 3.97 (4.11); **3**: C 46.98 (46.89), H 3.12 (3.37), N 3.94 (3.78); **4**: C 46.75 (46.61), H 3.10 (3.35), N 3.92 (4.07); **5**: C 46.54 (46.65), H 3.09 (3.32), N 3.90 (3.73); **6**: C 46.39 (46.23), H 3.08 (3.27), N 3.89 (4.05); **7**: C 46.02 (46.15), H 3.06 (3.29), N 3.86 (3.71); **8**: C 54.94 (54.83), H 3.65 (3.90), N 4.61 (4.76).

X-ray Crystallography and Structure Solution.

Data for **3**·4MeOH were collected at 180 K on a Stoe IPDS II area detector diffractometer using graphite-monochromated Mo-K*a* radiation, and were previously reported.[8]

Results and Discussion

Syntheses

The reaction between $M(NO_3)_3{\cdot}6H_2O$ (M= Gd, Tb, Dy, Ho, Er, Tm, Yb, Y) and LH_3 with aibH in 1:1:1 ratio in the presence of base under high pressure and high temperature conditions, afforded eight new homometallic clusters of the general formulae $[M^{III}_7(OH)_2(L')_9(aib)]{\cdot}4MeOH$ (Gd, **1**·4MeOH; Tb, **2**·4MeOH; Dy, **3**·4MeOH; Ho, **4**·4MeOH; Er, **5**·4MeOH; Tm, **6**·4MeOH; Yb, **7**·4MeOH, Y, **8**·4MeOH). To our surprise, the reaction formed in situ ligand L', upon the condensation of the naphthalene aldehyde with 2-amino-isobutyric acid. Furthermore, naphthalene aldehyde was used as a starting material for the synthesis of the LH_3 ligand, and our initial guess was that the LH_3 amount used in the reaction was "contaminated" by unreacted naphthalene aldehyde. Yet, ^{1}H-NMR, ^{13}C-NMR and ESI-MS studies of the LH_3 ligand used, clearly showed the absence of any unreacted aldehyde, suggesting that the formation of the ligand happened in situ. In order to test this hypothesis, we attempted to make the new ligand $L'H_2$ by trying two different approaches: i) upon reacting naphthalene aldehyde and aibH, and ii) upon reacting LH_3 with aibH. In both cases, we managed to observe the

formation of the L'H_2 ligand by means of ^{1}H-NMR and ES-MSI, but not as the solely product of the reaction, since a mixture of L'H_2 and unreacted starting materials was obtained. On the other hand, in the presence of the trivalent metal ions, the same two strategies form pure crystalline complexes **1**-**8**, in which only the L'H_2 ligand is found, suggesting that this transformation is metal-assisted. In order to see how the reaction's conditions affect the identity of the products, we performed various reactions by changing the metal:ligands ratio, the base used, as well as the time of the reaction, but in all cases the same heptanuclear clusters were obtained. The only synthetic parameters that affect the formation of the products are the high-temperature and high-pressure employed (solvothermal conditions), since under normal laboratory conditions no formation of any crystalline material was observed. Furthermore, repeating the same reactions in EtOH or MeCN produces no crystalline material. Finally, we managed to isolate the "medium-to-small" lanthanides' versions in terms of size, as well as the Y^{III} analogue, while in the case of the larger lanthanides (La^{III}-Eu^{III}) an amorphous solid was obtained that could not be further characterized. The identity of clusters **1**·4MeOH, **2**·4MeOH, **4**·4MeOH, **5**·4MeOH, **6**·4MeOH, **7**·4MeOH and **8**·4MeOH was established by means of i) pXRD comparison (Figs. 1 and S11) with the theoretical powder diffraction pattern of **3**·4MeOH, ii) C, H, N analysis, and iii) IR spectroscopy (Figure S12). Finally, we would like to mention that for all complexes reported we obtained large singe-crystals suitable for X-ray crystallography, but we felt it was unnecessary to proceed with single-crystal crystallography, since from all the above mentioned methods the identity of the clusters can be undoubtedly extracted.

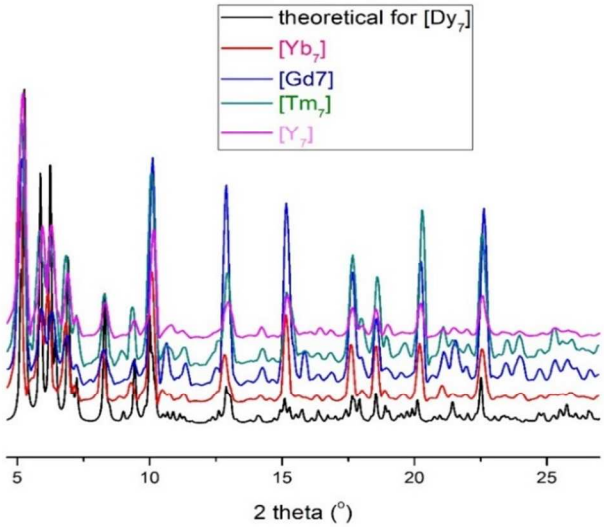

Figure 1. Powder XRD diagram comparison between the representative complexes **1**, **6**, **7**, **8** and **3** (theoretical diagram).

Description of structures

All **1**-**8** clusters are isostructural, and therefore only the structure of complex **3** is shown in Figure 2, while selected bond distances and angles are given in Table S1. Finally, only a short description of its structure is given since it has been described previously.[8] Complex **3** crystallizes in the triclinic space group *P*-1 and consists of a distorted octahedral [Dy_6] cage, which holds the seventh Dy^{III} atom in an off-centre manner towards the upper apex of the octahedron at a distance of ~ 1.3 Å from the basal plane of the octahedron. The nine L'$^{2-}$ dianions adopt three different coordination modes: i) two are found in an $\eta^2_{O\text{-hydroxyl}}$: η^1: η^1: η^1:μ_3 fashion, ii) six in an $\eta^2_{O\text{-carboxylate}}$: η^1: η^1: η^1:μ_3 mode, and iii) one in an η^1: η^1: η^1: η^1:μ fashion, while the unique aib$^-$ ligand is found in an η^1: η^1: η^1:μ mode forming a chelate ring via the –NH_2 group and one $O_{carboxylate}$ atom. The Dy^{III} centers are eight- and seven-coordinate, while a SHAPE analysis[9] yielded pentagonal bipyramidal geometry for Dy4, Dy5 and Dy7, triangular dodecahedral geometry for Dy6 and Dy2, and square antiprismatic geometry for Dy3 and Dy1.

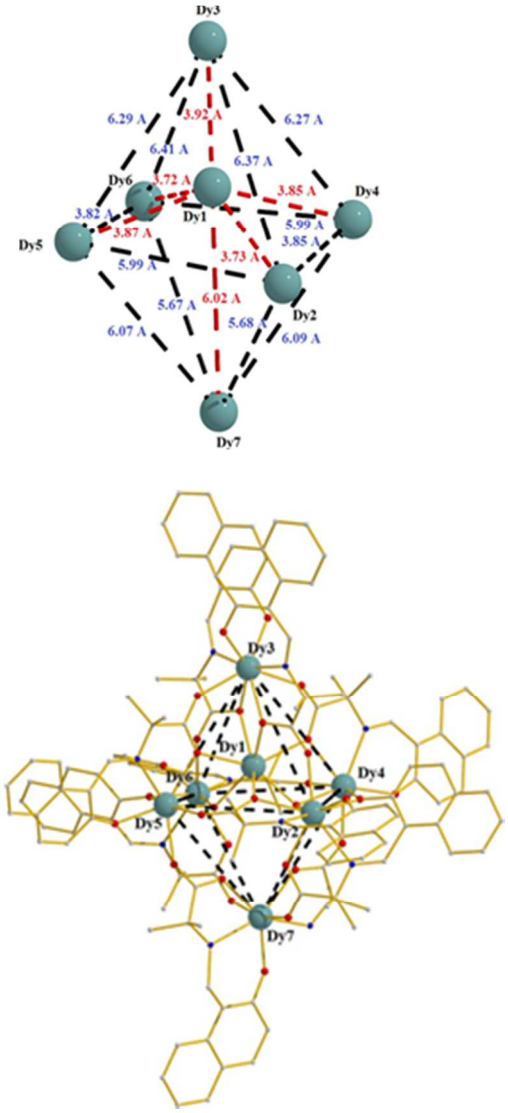

Figure 2. The molecular structure of **3** (bottom) along with its metallic dimensions (top). Hydrogen atoms and solvate molecules have been omitted for clarity. Color code: Dy^{III}= grey-blue, O= red, N= blue, C= grey.

Dc magnetic susceptibility studies

Direct current magnetic susceptibility measurements were performed on polycrystalline samples of all **1-7** complexes in the 5 – 300 K range under an applied field of 0.1 T. The results are plotted as the $\chi_M T$ product vs. T in Figure 3 (top), while in Table 1, the theoretical and the experimentally found $\chi_M T$ values at room temperatures for **1-7** are given for comparison. From a quick look it becomes apparent that all clusters present similar magnetic behavior; upon cooling- the $\chi_M T$ value decreases, suggesting the presence of antiferromagnetic interactions and/or depopulation of the Stark sublevels of the 4*f* ions. Furthermore, from the line-shape of the $\chi_M T$ vs. T curve for the [Gd_7] cluster it becomes apparent that the antiferromagnetic interactions present are weak, since the room temperature $\chi_M T$ value remains almost constant until ~ 40 K, as expected due to the inner nature of the 4*f* electrons. In addition, the existence of antiferromagnetic interactions may be further supported from a Curie-Weiss analysis of the high temperature (40 – 300 K) magnetic susceptibility data for all complexes, yielding negative θ values (Figure 4, top), *albeit* such analysis does not exclude the effect of the depopulation of the Stark sublevels. Actually, given that all clusters are isostructural, and the presence of very weak interactions for the [Gd_7] analogue (*vide infra*), the Curie-Weiss analysis should be "dominated" by the depopulation of the Stark sub-levels and not by the nature of the dominant exchange interactions, so it should be treated with caution.

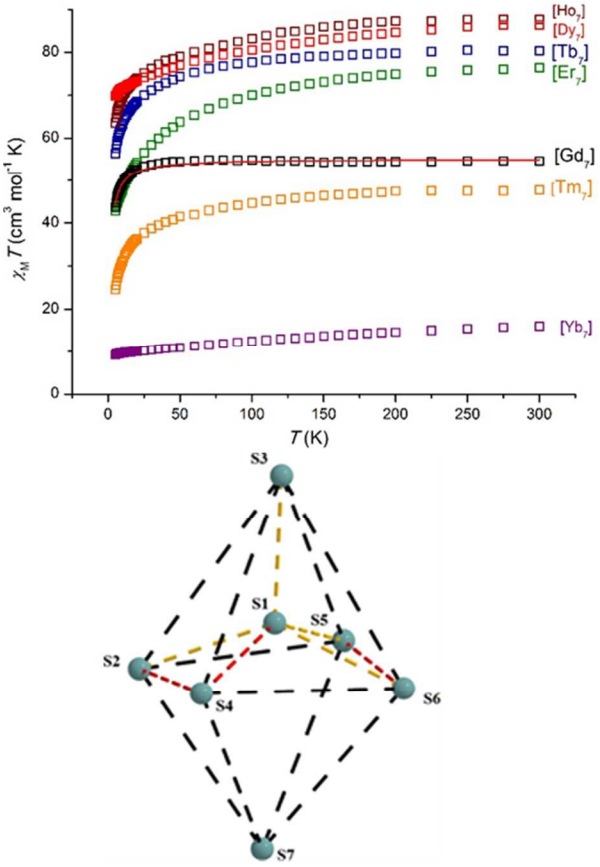

Figure 3. Plot of $\chi_M T$ vs. T for complexes **1-7** under an applied dc field of 1000 G (top); exchange interaction scheme for complex **1**, displaying J_1 (black dotted lines), J_2 (red dotted lines) and J_3 (orange dotted lines) (bottom); see text for details.

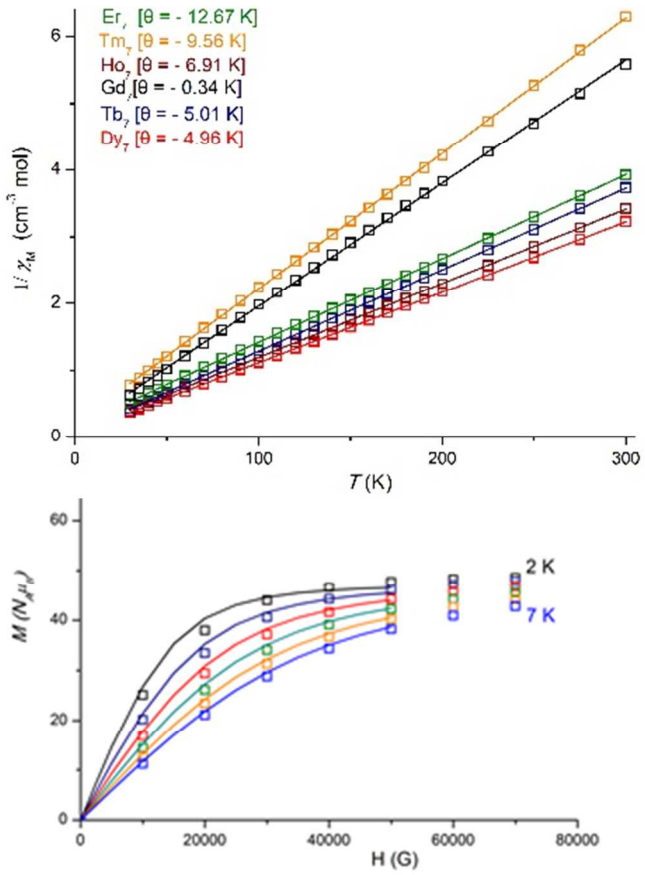

Figure 4. Curie-Weiss plot for complexes **1**-**6** for the 50 – 300 K range (top); M vs. H for **1** in the 1 – 7 T and 2.0 – 7.0 K field and temperature range (bottom). The solid lines represent simulation of the magnetization isotherms in the 1-5 T field range and 2-7 K temperature range (top-to-bottom), assuming the parameters obtained from the dc susceptibility simulation (see text for details).

We were able to successfully simulate the $\chi_M T$ data for the [Gd_7] cluster adopting a 3-*J* model (Figure 3, bottom) and the Hamiltonian equation (1), which assumes the following exchanges interactions: i) one exchange, J_1, between Gd3-Gd2, Gd3-Gd4, Gd3-Gd5, Gd3-Gd6, Gd7-Gd4, Gd7-Gd2, Gd7-Gd5, Gd7-Gd6, Gd4-Gd6 and Gd2-Gd5, mediated by one *syn,anti* carboxylate ligand at ~6 Å apart, ii) one J_2 between Gd2-Gd4, Gd6-Gd5 and Gd1-Gd4 mediated by two monoatomic alkoxide bridges at ~ 4 Å apart, and iii) one J_3 between Gd1-Gd2, Gd1-Gd5, and Gd1-Gd6, mediated by two monoatomic alkoxide and one syn,syn carboxylate bridges, andbetween Gd1-Gd3 mediated by two monoatomic alkoxide and two syn,syn carboxylate bridges. Using the new and powerful program PHI,[10] and employing the Hamiltonian in eqn (1)

$$\hat{H} = -2J_1 (\hat{S}_3\hat{S}_2 + \hat{S}_3\hat{S}_4 + \hat{S}_3\hat{S}_5 + \hat{S}_3\hat{S}_6 + \hat{S}_7\hat{S}_4 + \hat{S}_7\hat{S}_2 + \hat{S}_7\hat{S}_5 + \hat{S}_7\hat{S}_6 + \hat{S}_4\hat{S}_6 + \hat{S}_2\hat{S}_5) - 2J_2 (\hat{S}_2\hat{S}_4 + \hat{S}_6\hat{S}_5 + \hat{S}_1\hat{S}_4) - 2J_3 (\hat{S}_1\hat{S}_2 + \hat{S}_1\hat{S}_5 + \hat{S}_1\hat{S}_6 + \hat{S}_1\hat{S}_3) \quad (1)$$

afforded the parameters J_1 = -0.011 cm^{-1}, J_2 = -0.030 cm^{-1}, J_3= -0.020 cm^{-1} and g = 2.00. These parameters lead to the S=1/2, 3/2, 5/2 and 7/2 spin-states located within only ~0.1 cm^{-1}, with the S=3/2 located marginally lower than the others. Furthermore, these J values are in excellent agreement with previously reported Gd^{III} systems,[11] while finally the system may be regarded as "simply paramagnetic", given the very small exchange interactions present.

Magnetization data were collected for **1** in the magnetic field and temperature ranges of 1 – 7 T and 2.0 – 7.0 K, but we could not obtain a good fit for the data assuming that only the ground state is populated. The magnetization at 2 K saturates rapidly to 47.3 Bohr magnetons, and we managed to simulate the M vs. H data with the parameters obtained from the *dc* susceptibility measurements (Figure 4, bottom).

Table 1. Theoretical and experimentally found $\chi_M T$ values (cm^3 mol^{-1} K) for 1-7 (at 300 K).

Complex	g_j	$\chi_M T$ theor.	$\chi_M T$ exper.
[Gd_7] (**1**)	2.00	55.12	53.71
[Tb_7] (**2**)	1.50	82.68	80.36
[Dy_7] (**3**)	1.33	99.16	86.41
[Ho_7] (**4**)	1.25	98.43	87.66
[Er_7] (**5**)	1.20	80.32	76.42
[Tm_7] (**6**)	1.17	50.02	47.67
[Yb_7] (**7**)	1.14	18.00	16.01

Ac Magnetic Susceptibility Studies

Ac magnetic susceptibility measurements were performed on polycrystalline samples of complexes **2**·4MeOH, **3**·4MeOH and **5**·4MeOH in the 1.8 – 10 K range in zero applied dc field and 2.5 G ac field oscillating at 100 – 1500 Hz range. For all three samples measured the in-phase (χ_M', plotted as χ_M'T vs. T, Figures S1-3) signal decreases upon decreasing temperature, indicating the presence of low-lying excited states with larger "S" values than the "ground-state", in agreement with the dominant antiferromagnetic interactions qualitatively found from the Curie-Weiss analysis; yet again, the depopulation of the Stark sublevels should not be excluded from the interpretation of the curves. Furthermore, only the Dy^{III} analogue displays frequency and temperature-dependent out-of-phase (χ_M'') signals below ~ 3 K, but no peaks are seen (Figure S4), indicating the possibility of Single Molecule Magnetism behavior, albeit with a small barrier to magnetization reversal. In order to fully prove the SMM character of **3**·4MeOH, single-crystal hysteresis measurements should be performed, but given its potential small U_{eff} we chose not to perform such measurements, since nowadays there are many SMMs with small-moderate U_{eff} values. In order to investigate the origin of the small barrier for the relaxation of the magnetization, we performed ac measurements in the presence of an applied dc field, as a means of quenching the quantum tunneling of magnetization (QTM) possibly present which drastically diminishes U to its U_{eff} value; a method currently revitalized,[12] although firstly established many years ago.[13] Indeed, upon employment of various dc fields we noticed the appearance of χ_M'' peaks, that shifted to higher temperatures upon increasing the applied dc field (Figure 5), thus proving the presence of QTM. Yet, this result should be taken with caution, since the appearance of χ_M'' peaks upon applying dc fields during ac measurements does not always guarantee proof of SMM behavior, especially in the cases where no χ_M'' signals are observed upon zero dc field.[14] Therefore, we did not perform ac measurements under various dc fields for clusters **2**·4MeOH and **5**·4MeOH, since they do not display out-of-phase signals in the absence of an external dc field.

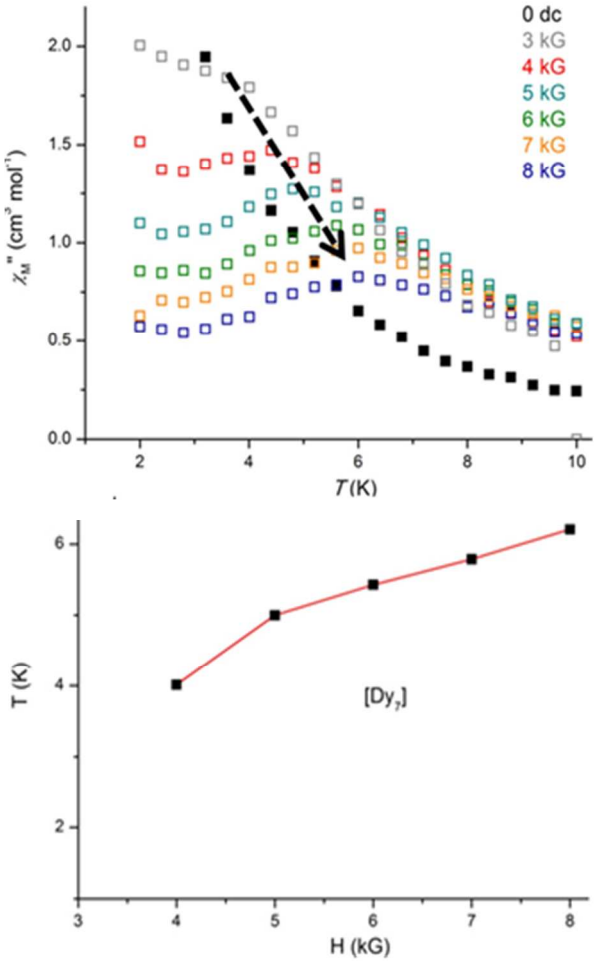

Figure 5. Plot of the out-of-phase (χ_M'') signal *vs.* temperature for **3** in a 2.5 G field oscillating at 1500 Hz frequency under various applied dc fields; the arrow shows the shift of the χ_M'' maximum (top); the shift of the χ_M'' maximum at higher temperatures as a function of the applied dc field.

A detailed CCDC search revealed that clusters **1**-**7** join a small family of heptanuclear [Ln$^{III}_7$] complexes that contains nine sub-categories (Table 2), with the most magnetically interesting being cluster [$Dy_7(OH)_6(thmeH_2)_5(thmeH)(tpa)_6(MeCN)_2](NO_3)_2$ ($thmeH_3$: tris(hydroxymethyl) ethane, tpaH: triphenylacetic acid) which functions as a SMM with a large

energy barrier for the reorientation of the magnetization of 140 K.[21]

Complex	Ref.
$[(HO)_9(H_2O)Eu_7(calix[9]arene6H)_2(DMSO)_6]$	16
$[Sm_7S_7(SePh)_6(DME)_7][Hg_3(SePh)_7]$	17
$[Dy_7(\mu_3\text{-}OH)_5(MeOsalox)_2(MeOsaloxH)_4(PhCO_2)_7(OH)(H_2O)_{1.5}(MeOH)_{0.5}]$	18
$[Eu(EuL2)_6](OTf)_9$	19
$[La_7\{(S)\text{-}L\}_6(CO_3)(NO_3)_6(OCH_3)(CH_3OH)_7]$	20
$[Gd_7(OH)_6(thmeH_2)_5(thmeH)(tpa)_6(MeCN)_2](NO_3)_2$	21
$[Dy_7(OH)_6(thmeH_2)_5(thmeH)(tpa)_6(MeCN)_2](NO_3)_2$	21
$[Eu(EuL_2)_6](OTf)_9$	22
$[Nd(NdL_2)_6](OTf)_9$	22
$[Dy^{III}_7(OH)_2(L')_9(aib)]$	8, t.w.
$[Gd^{III}_7(OH)_2(L')_9(aib)]$	t.w.
$[Tb^{III}_7(OH)_2(L')_9(aib)]$	t.w.
$[Ho^{III}_7(OH)_2(L')_9(aib)]$	t.w.
$[Er^{III}_7(OH)_2(L')_9(aib)]$	t.w.
$[Tm^{III}_7(OH)_2(L')_9(aib)]$	t.w.
$[Yb^{III}_7(OH)_2(L')_9(aib)]$	t.w.
$[Y^{III}_7(OH)_2(L')_9(aib)]$	t.w.
$[Dy_7(TBC[8]\text{-}7H)(TBC[8]\text{-}6H)(\mu_4\text{-}O)_2(\mu_3\text{-}OH)_2(\mu_2\text{-}OH)_2(dmf)_9]$	23

Table 2. Structurally characterized heptanuclear homometallic $[Ln^{III}_7]$ clusters.

p-t-Bu-calix[9]arene, DME: dimethoxyethane, $MeOsaloxH_2$: 3-methyloxysalicylaldoxime, HL: 2,2′:6′,2″-terpyridine-6-carboxylic acid, (S)-H_2L: (S)-2-(2-hydroxybenzylamino)-3-carbamoylpropanoic acid, $thmeH_3$: tris(hydroxymethyl)ethane, tpaH: triphenylacetic acid, LH_3:2-(β-naphthalideneamino)-2-(hydroxymethyl)-1-propanol, aibH: 2-aminoisobutyric acid, TBC[8]:p-tert-Butylcalix[8]arene

Thermal decomposition properties

In order to investigate the thermal stability of the heptanuclear species, thermogravimetric analyses (TGA) were carried out on freshly made polycrystalline samples of **1**·4MeOH, **3**·4MeOH and **7**·4MeOH. The thermal decomposition of both complexes is the same (Figure 6); it starts with an extended plateau in the 100-340°C indicating a thermostable product, while above ~340ºC, the complexes quickly decompose displaying a ~35% mass-loss, indicating the loss of almost all organic matter, leading to the formation of metal-oxides species. We did not observe the loss of the four MeOH co-crystallized solvate molecules, possibly because the samples become "de-solvated" upon standing on air before the start of the measurement.

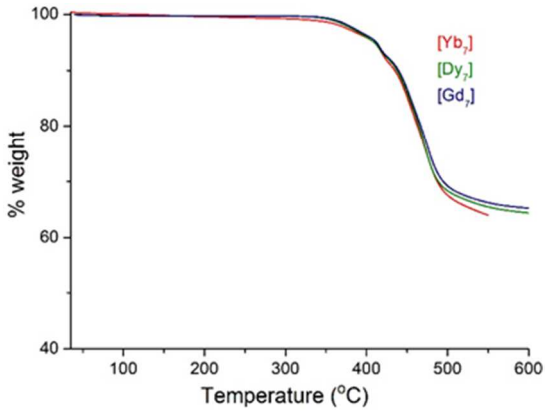

Figure 6. Thermogravimetric analyses of complexes **1**·4MeOH, **3**·4MeOH and **7**·4MeOH in the 40-600 °C temperature range.

NMR studies

In order to investigate the solution stability of the clusters, we performed various NMR measurements on the diamagnetic analogue, $[Y^{III}_7(OH)_2(L')_9(aib)]$·4MeOH (**8**·4MeOH) in $CDCl_3$. ^1H NMR spectra of **8**·4MeOH remained unchanged after leaving the $CDCl_3$ solution at room temperature under ambient light for at least two weeks (Figure S5). 2D DOSY experiments using the Stimulated Echo pulse sequence performed in two different NMR spectrometers indicated that the solution contained only one species, with a diffusion coefficient of ~ 4.0 x 10-10 m^2/s. (Figure S6).[24] Using the Stokes-Einstein equation this value represents a species with a hydrodynamic radius of ~10 Å in solution, in excellent agreement with the crystallographic data for the Dy^{III} analogue (~ 11-12 Å), indicating that 8 retains its structural integrity in solution. This was further elucidated with the use of homonuclear and heteronuclear 2D NMR spectroscopy (Figures S7-S9); the ^1H NMR spectrum of **8**·4MeOH has excellent resolution (see Figure S5), and each of the protons 1-9 and 12, 12' (Scheme 1) produces five different peaks, indicating the presence of five different environments for L' ligands, named a-e (*vide infra*, Figure 8). Integration of the respective proton peaks shows that there is one b-type ligand L', but two L's for types a, c, d, and e, in accordance with what is expected from the X-ray structure of **8**, in which the metal ions are bound with nine L' ligands and one aib ligand. The aib ligand of **8** is also present and its protons are assigned in the ^1H NMR spectrum of **8** in $CDCl_3$. The complete assignment of the proton and carbon signals of **8** in $CDCl_3$ was accomplished by using a variety of homonuclear (gCOSY, gTOCSY) and heteronuclear (gHSQC, gHMBC) 2D NMR experiments. As a representative example, figure 7 depicts the aromatic region of the 2D ^1H-^{13}C heteronuclear correlation HSQC spectrum of **8**, indicating the assignment of

protons 1-9 in the five different types of L' ligands. The total assignment of the NMR spectra of **8** is presented in Table S2.

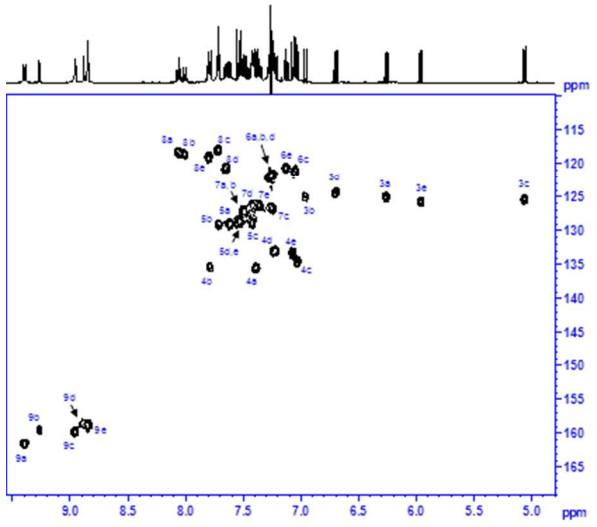

Figure 7. Aromatic region of the 2D ^{1}H-^{13}C heteronuclear HSQC spectrum of **8** in $CDCl_3$ solution. Labels indicate the assignment of protons 1-9 in ligands L' of type **a**-**e**.

Inspection of the chemical shifts reported in Table S3 shows that the largest spread in proton shifts is observed for H-3 ($\Delta\delta$ = 1.9), followed by H-4 ($\Delta\delta$ = 0.76) and H-9 ($\Delta\delta$ = 0.56). These protons are located very close to the complexation points of the aromatic ligands with Y, and thus are expected to be most heavily affected by electron density changes, compared to the free ligand. The methyl H-12 and H-12' protons of the L' ligands also show a rather large chemical shift dispersion of ~ 1.0 ppm, however in this case this is probably attributed to conformational reasons and not electron density differences. A detailed study of the ^{1}H and ^{13}C NMR chemical shift dispersion characteristics of ligands L' in **8**, in conjunction with theoretical NMR calculations is under way.

After successfully assigning the protons of **8**, a 2D NOESY experiment was performed, to obtain information on the relative proximity in space of protons belonging to different L' ligands, based on their NOE enhancement (Figure S9). Strong intramolecular NOEs were observed between protons H-8, H-9 and H-12/H12' belonging to the same ligand (type *a*-*e*), as expected from the solid-state structure of **3**. However, several strong inter-ligand NOEs (between protons not belonging to the same L') were also observed, and are reported in Table 4, together with the respective proton-proton distances obtained from the X-ray crystal structure of **3**. It should be noted that due to extensive resonance between the aromatic rings and the side chain of the L' ligands, the complex is expected to retain high levels of rigidity in solution, with negligible motional freedom regarding ring rotation. This is in accordance with the fact that the majority of solution NOEs reported in Table S3 represent crystal structure H-H distances between 3 and 4 Å, with only a handful between 4 and 5 Å. The large NOEs observed between H-3a and the side chain methyl groups H-12 of aib and ligand *b* (aib and *b* are connected to Y-7) identifies the two equivalent ligands *a* (coloured magenta in Figure 8). Extensive NOEs between H-9*a* and H-12*a* and protons of the *d* aromatic ring (3*d*, 4*d*) helped identify *d* (yellow in Figure 8) as the next neighbour of *a*, while NOEs between H-12*d* protons and H-9*c* identified *c* as the two remaining L' type ligands (green) on the basal plane of the structure. The H-12*e* methyl group protons show large NOEs with both 3*d* and 3*c* protons, indicating two *e* L's connected to Y3 on the "top" of the structure of **8**. Finally, NOEs observed between H-9*b* and H-12*b* verify the assignment of the single *b* type ring to that at the bottom of the structure next to aib, complexing with Y-7. In summary, the NMR results presented, convincingly prove that complex **8** is very stable and retains its structure in $CDCl_3$ solution at least for a period of two weeks. This result is in full agreement with the lack of change in its UV-vis and emission characteristics/pattern (*vide infra*) in going from the solid state to solution.

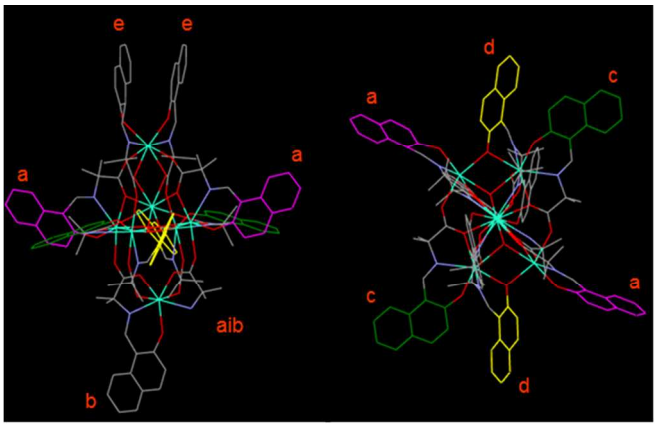

Figure 8. Assignment of the five types of L' ligands of **8** in $CDCl_3$ solution based on NOE experiments. Left: side view, right top view.

Absorption and emission spectroscopy

The solid-state electronic absorption spectra of all complexes were recorded, and found to display the same pattern as expected. In Figure 9, the solid-state absorption spectra of clusters **3**·4MeOH ([Dy_7]), **4**·4MeOH ([Ho_7)], **6**·4MeOH ([Tm_7]) and **7**·4MeOH ([Yb_7]), as well of the LH_3 are shown, while for comparison the solid-state and solution absorption spectra for the [Dy_7] analogue are displayed. From Figure 9, three main results can be extracted: i) all spectra display ligand-dominated peaks, ii) the absorbance peaks of the free ligand are "blue" shifted when bound in the complexes, with the peaks at 404 and 428 nm shifted at 382 and 400 nm, *.i.e.* 22 and 28 nm, respectively, and iii) the solid-state and solution spectra are identical as expected since the species are stable in solution, with the only difference being the "narrowing" of the peaks in solution with respect to the "broadening" in solid-state, due to collisional broadening. In Figure 10, the solid-state room

temperature fluorescence emission spectra for LH_3 and complex **3** are given, as well as the solid-state emission for **3** at various wavelengths, while in Figure 11 the solution emission and excitation spectra of complex **3** in $CHCl_3$ are shown. Complex **3** strongly emits blue light displaying a peak at 467 nm, while in addition another peak at 559 nm, *albeit* much weaker, exists. In order to see whether all peaks are due to emission transitions, we repeated the solid-state emission of **3** at various excitation wavelengths (Figure 10), and we can see that the peak at 559 nm is not "real", while both additional peaks at 481 and 492 nm are real and due to emission transitions, but are difficult to assign at this stage.

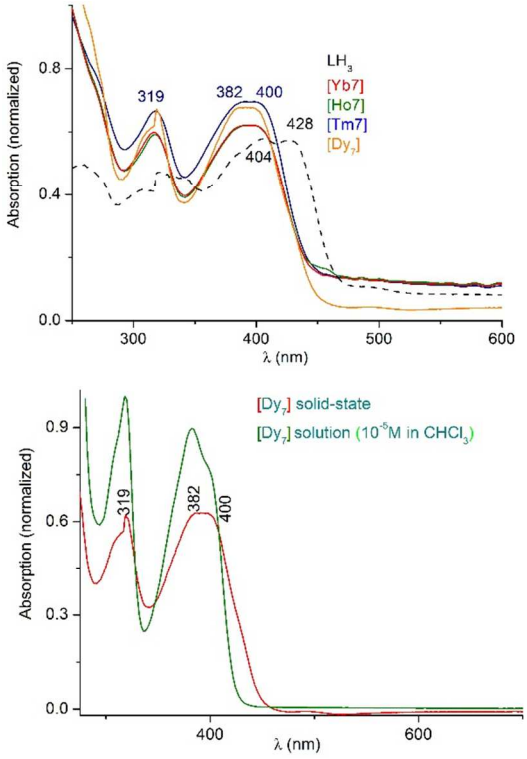

Figure 9. Solid-state Uv-vis spectra of LH_3 (dashed-line) and complexes **3**·4MeOH, **4**·4MeOH, **6**·4MeOH and **7**·4MeOH (top); comparison of solid-state and solution (10^{-5} M in $CHCl_3$) UV-Vis spectra for **3**·4MeOH (bottom).

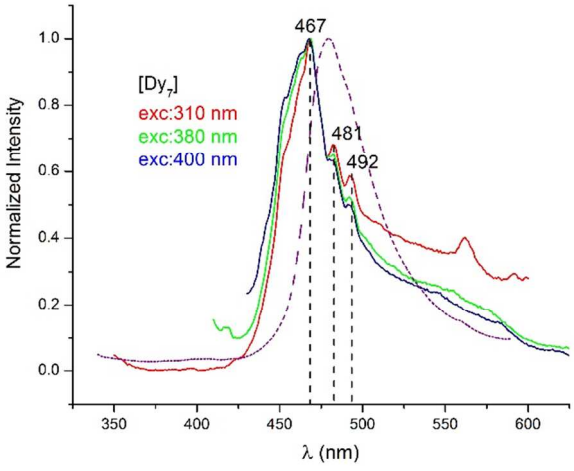

Figure 10. Solid-state room temperature emission spectra for **3** with excitation wavelength at 310, 380 and 400 nm and LH_3 (purple dotted line) with excitation wavelength at 310 nm.

Finally, in order to check whether the emission is ligand- or lanthanide-based, we performed solid-state fluorescence studies at complexes **4** ($[Ho^{III}_7]$) and **7** ($[Yb^{III}_7]$) which are shown in Figure S10. Upon spectra comparison of these analogues, we see that all complexes display the same pattern, emitting in the 455-467 blue-light region. Furthermore, the pattern of the spectra is the same for all clusters studied, therefore, establishing that the emission is ligand-based. Finally, for cluster **3**, the quantum yield of the complex was found to be Φ= 0.0001 (=0.1%) while the calculation was based on anthracene (Φ=0.27 in ethanol).[25]

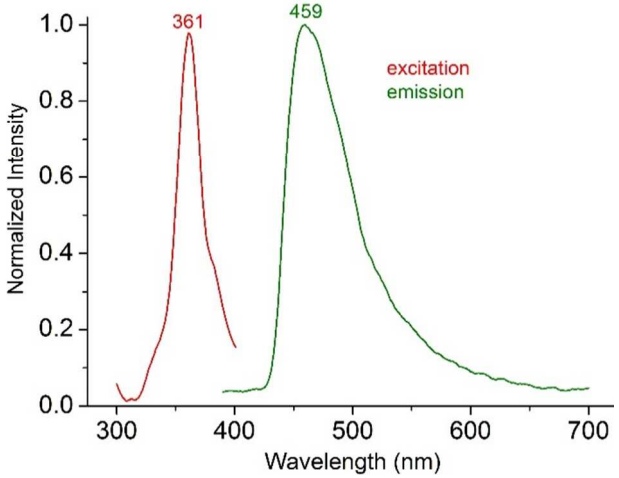

Figure 11. Solution emission spectrum for **3** in $CHCl_3$ (10^{-4} M) upon excitation at 360 nm (green line); excitation spectrum of **3** in $CHCl_3$ (10^{-4} M) monitoring the emission at 459 nm (red line).

Conclusions

In conclusion, we have reported the syntheses, structures, magnetic properties, absorption-emission properties and thermal stability of seven new homometallic lanthanide heptanuclear $[Ln^{III}_7]$ complexes based on the use of LH_3 (2-(β-naphthalideneamino)-2-hydroxymethyl-1-propanol) and aibH (2-amino-isobutyric acid) in 4*f* chemistry. Furthermore, we reported the synthesis and studies of the diamagnetic $[Y^{III}_7]$ analogue, which served as a probe in order to investigate the solution stability of the species *via* extended 1D and 2D NMR studies.

Amongst all clusters studied, complex $[Dy^{III}_7]$ (**3**) was found to display out-of-phase ac signals, suggesting the possibility of SMM behavior, while in addition it emits blue-light upon excitation at various wavelengths, as is the case for the other heptanuclear clusters as well. Furthermore, the clusters retain their structural integrity in solution ($CHCl_3$) as was evidenced by the NMR studies performed in the diamagnetic Y^{III} analogue, while finally, all clusters are thermally stable up to ~

340°C, a remarkable feature for any polynuclear metallic complex. To the best of our knowledge cluster **3** is the first example of any polynuclear lanthanide cluster combining: i) potential SMM behavior, ii) emission properties, iii) solution stability, and iv) thermal stability up to 340°C.

Work is currently underway towards the isolation of "analogous" complexes by employing various aldehydes as starting materials in order to generate new Schiff bases *in situ*, and thus affect the identity of the products.

Acknowledgements

CJM and ABC: "This research has been co-financed by the European Union (European Social Fund – ESF) and Greek national funds through the Operational Program "Education and Lifelong Learning" of the National Strategic Reference Framework (NSRF) - Research Funding Program: THALES. Investing in knowledge society through the European Social Fund".

Notes and references

[a] Department of Chemistry, The University of Crete, Voutes, 71003, Herakleion, Greece.

[b] Institute of Electronic Structure and Laser, Foundation for Research and Technology-Hellas (IESL-FORTH), P.O. Box 1385, GR 711 10 Herakleion, Crete, Greece.

† Footnotes should appear here. These might include comments relevant to but not central to the matter under discussion, limited experimental and spectral data, and crystallographic data.

Electronic Supplementary Information (ESI) available: Bond distances and angles for **3**, magnetic data for clusters **2**, **3** and **5**, as well as a complete series of 1D and 2D NMR spectra for **8**. See DOI: 10.1039/b000000x/

1 See for example: J. -C. G. Bünzli and C. Piguet, *Chem. Soc. Rev*., 2005, **34**, 1048; K. Binnemans, *Chem. Rev*., 2009, **109**, 4283.

2 Representative references and refs therein: G. Christou, D. Gatteschi, D. N. Hendrickson and R. Sessoli, *Mater. Res. Bull.* 2000, **25**, 66; R. Sessoli and D. Gatteschi, *Angew. Chem. Int. Ed.* 2003, **42**, 268; G. Aromí and E. K. Brechin, *Structure and Bonding* 2006, **122**, 1; R. Bagai and G. Christou, *Chem. Soc. Rev.* 2009, **38**, 1011; A. Dei and D. Gatteschi, *Angew. Chem. Int. Ed.* 2011, **50**, 11852; R.E.P. Winpenny, (Ed.), Single-Molecule Magnets and Related Phenomena, *Structure and Bonding* 2006, volume **122**; L. Sorace, C. Benelli and D. Gatteschi, *Chem. Soc. Rev*. 2011, **40**, 3092; F. Habib and M. Murugesu, *Chem. Soc. Rev.* 2013, **42**, 3278.

3 N. Ishikawa, M. Sugita, T. Ishikawa, S. Koshihara and Y. Kaizu, *J. Am. Chem. Soc*. 2003, **125**, 8694.

4 For excellent recent reports on 4*f* SMMs see: D. N. Woodruff, R. E. P. Winpenny and R. A. Layfield, *Chem. Rev.* 2013, **113**, 5110; R. Sessoli and A. K. Powell, *Coord. Chem. Rev.* 2009, **253**, 2328; J. D. Rinehart and J. R. Long, *Chem. Sci.* 2011, **2**, 2078; Y. -N. Guo, G. -F. Xu, Y. Guo and J. Tang, *Dalton Trans*. 2011, **40**, 9953; P. Zhang, Y.-N. Guo and J. Tang, *Coord. Chem. Rev.* 2013, **257**, 1728; Y.-N. Guo, G.-F. Xu, P. Gamez, L. Zhao, S.-Y. Lin, R. Deng, J. Tang and H.-J. Zhang, *J. Am. Chem. Soc.* 2010, **132**, 8538; Y.-N. Guo, G.-F. Xu, W. Wernsdorfer, L. Ungur, Y. Guo, J. Tang, H.-J. Zhang, L. F. Chibotaru and A. K. Powell, *J. Am. Chem. Soc*. 2011, **133**, 11948.

5 M. Gonidec, R. Biagi, V. Corradini, F. Moro, V. De Renzi, U. Pennino, D. Summa, L. Muccioli, C. Zannoni, D. B. Amabilino and J. Veciana, *J. Am. Chem. Soc*. 2011, **133**, 6603.

6 R. J. Blagg, L. Ungur, F. Tuna, J. Speak, P. Comar, D. Collison, W. Wernsdorfer, E. J. L. McInnes, L. F. Chibotaru and R. E. P. Winpenny, *Nature Chem.* 2013, **5**, 673.

7 M. Orfanoudaki, I. Tamiolakis, M. Siczek, T. Lis, G. S. Armatas, S. A. Pergantis and C. J. Milios, *Dalton Trans*. 2011, **40**, 4793.

8 A. B. Canaj, D. I. Tzimopoulos, A. Philippidis, G. E. Kostakis and C. J. Milios, *Inorg. Chem.* 2012, **51**, 7451.

9 M. Llunell, D. Casanova, J. Girera, P. Alemany and S. Alvarez, SHAPE, version 2.0, Barcelona, Spain 2010.

10 N. F. Chilton, R. P. Anderson, L. D. Turner, A. Soncini and K. S. Murray, *J. Comput. Chem.* 2013, **34**, 1164.

11 See for example: C. A. Black, J. S. Costa, W. T. Fu, C. Massera, O. Roubeau, S. J. Teat, G. Aromi, P. Gamez and J. Reedijk, *Inorg. Chem.* 2009, **48**, 1062; J. D. Rinehart, M. Fang, W. J. Evans and J. R. Long, *Nature Chem.,* 2011, **3**, 538; A. Panagiotopoulos, T. F. Zafiropoulos, S. P. Perlepes, E. Bakalbassis, I. Massonramade, O. Kahn, A. Terzis and C. P. Raptopoulou, *Inorg. Chem.* 1995, **34**, 4918; L. E. Roy and T. Hughbanks, *J. Am. Chem. Soc.* 2006, **128**, 568.

12 See for example: V. Chandrasekhar, B. M. Pandian, J. J. Vittal and R. Clérac, *Inorg. Chem*. 2009, **48**, 1148; W. Harman, T. D. Harris, D. E. Freedman, H. Fong, A. Chang, J. D. Rinehart, A. Ozarowski, M. T. Sougrati, F. Grandjean, G. J. Long, J. R. Long and C. J. Chang, *J. Am. Chem. Soc.* 2010, **132**, 18115; T. Jurca, A. Farghal, P. -H. Lin, I. Korobkov, M. Murugesu and D. S. Richeson, *J. Am. Chem. Soc*. 2011, **133**, 15814; D. E. Freedman, W. H. Harman, T. D. Harris, G. J. Long, C. J. Chang and J. R. Long, *J. Am. Chem. Soc*. 2010, **132**, 1224; J. M. Zadrozny and J. R. Long, *J. Am. Chem. Soc*. 2011, **133**, 20732; J. Vallejo, I. Castro, R. Ruiz-García, J. Cano, M. Julve, F. Lloret, G. D. Munno, W. Wernsdorfer and E. Pardo, *J. Am. Chem. Soc.* 2012, **134**, 15704.

13 S. L. Castro, Z. Sun, C. M. Grant, J. C. Bollinger, D. N Hendrickson, G. Christou, *J. Am. Chem. Soc.* 1998, **120**, 2365; J. M. Hernández, X. X. Zhang, F. Luis, J. Bartolomé, J. Tejada and R. Ziolo, *Europhys. Lett*. 1996, **35**, 301.

14 Y. Sanakis, M. Pissas, J. Krzystek, J. Telser and R. G. Raptis, *Chem. Phys. Lett.* 2010, **493**, 185.

15 E. Lucaccini, L. Sorace, M. Perfetti, J. -P. Costes and R. Sessoli, *Chem. Commun*. 2014, **50**, 1648.

16 S. Fleming, C. D. Gutsche, J. M. Harrowfield, M. I. Ogden, B. W. Skelton, D. F. Stewart and A. H. White, *Dalton Trans.* 2003, 3319.

17 D. Freedman, T. J. Emgea and J. G. Brennan, *J. Am. Chem. Soc*. 1997, **119**, 11112.

18 F. -S. Guo, P. -H. Guo, Z. -S. Meng and M. –L. Tong, *Polyhedron*, 2011, **30**, 3079.
19 Y. Bretonniere, M. Mazzanti, J. Pecaut and M. M.Olmstead, *J. Am. Chem. Soc*. 2002, **124**, 9012.
20 X. -L. Tang, W.-H. Wang, W. Dou, J. Jiang, W. -S. Liu, W. -W. Qin, G. -L. Zhang, H. -R. Zhang, K. -B. Yu and L.-M. Zheng, *Angew. Chem.,Int. Ed*. 2009, **48**, 3499.
21 J. W. Sharples, Y.-Z. Zheng, F. Tuna, E. J. L. McInnes and D. Collison *Chem. Commun.* **2011**, *47*, 7650.
22 X.-Y. Chen, Y. Bretonniere, J. Pecaut, D. Imbert, J. -C. Bunzli and M. Mazzanti, *Inorg. Chem.* 2007, **46**, 625.
23 S. M. Taylor, S. Sanz, R. D. McIntosh, C. M. Beavers, S. J. Teat, E. K. Brechin and S. J. Dalgarno *Chem.-Eur. J.* 2012, **18**, 16014.
24 For NMR and diffusion studies of other Y complexes, see for example: D. T. Thielemann, I. Fernández and P. W. Roesky, *Dalton Trans.* 2010, **39**, 6661; M. W. Löble, M. Casimiro, D. T. Thielemann, P. Oña-Burgos, I. Fernández, P. W. Roesky and F. Breher, *Chem.-Eur. J.* 2012, **18**, 5325.
25 W. H. Melhuish, *J. Phys. Chem.* 1961, **65**, 229.

A family of heptanuclear lanthanide [Ln_7] complexes were isolated and fully characterized by magnetic measurements, NMR and absorption-emission spectroscopy.